Int. J. Electrochem. Sci., 13 **(2018)** 3441 – 3451, doi: 10.20964/2018.04.37

International Journal of
ELECTROCHEMICAL
SCIENCE
www.electrochemsci.org

Short Communication

Facile Hydrothermal Synthesis of Sulphur/Boron-doped Reduced Graphene Oxide Composite Cathodes for High-Performance Li/S Batteries

Yuan Tian[1], *Chenglong Deng*[1], *Zhenghao Sun*[1], *Yan Zhao*[1*], *Taizhe Tan*[2], *Fuxing Yin*[1*], *Xin Wang*[3*]

[1] School of Materials Science & Engineering, Research Institute for Energy Equipment Materials, Tianjin Key Laboratory of Materials Laminating Fabrication and Interface Control Technology, Hebei University of Technology, Tianjin 300130, China
[2]Synergy Innovation Institute of GDUT, Heyuan, Guangdong Province, China
[3]South China Academy of Advanced Optoelectronics, South China Normal University, Guangzhou 510006, China
[*]E-mail: yanzhao1984@hebut.edu.cn; yinfuxing@hebut.edu.cn; wangxin@scnu.edu.cn

Received: 12 December 2017 / *Accepted:* 13 February 2018 / *Published:* 6 March 2018

A sulphur/boron-doped reduced graphene oxide (S/B-rGO) composite was prepared using a facile hydrothermal method. The two-dimensional stacked nanosheet structure of the S/B-rGO composite provides an effective electron-conduction path and traps soluble polysulphide intermediates via the introduction of boron doping. The electrochemical performance delivers a relatively high reversible discharge capacity of 521.9 mAh g^{-1} after 100 cycles at 0.1 C with a boron-doped reduced graphene oxide composite lithium/sulphur battery.

Keywords: lithium/sulphur battery, sulphur/boron-doped reduced graphene oxide (S/B-rGO) composite, cathode material, hydrothermal synthesis.

1. INTRODUCTION

Lithium/sulphur (Li/S) batteries have received much attention due to their attractive ultrahigh theoretical capacity (1675 mAh g^{-1}), natural abundance, low cost and the environmental safety of sulphur[1-6]. There remain thorny issues hindering the use of Li/S batteries: the insulation by sulphur, the dissolution of the intermediate lithium polysulphide discharge products in the electrolyte, and the volume change within the cathode [7].

To solve these problems, the combination of sulphur with carbon-based materials, as in carbon nanotubes [8-9], carbon nanofibres [10], micro/mesoporous carbon [11-13] and graphene [14-18] has

been widely used to improve the electrochemical performance of Li/S batteries. Among these carbon-based materials, graphene is the most efficient sulphur host material due to its large specific area, high conductivity, good chemical stability and strong mechanical strength. Konarov's group [19] reported that the S/dehydrogenated polyacrylonitrile/rGO composite is used as cathode material for Li/S batteries. This composite shows excellent rate performance, delivering a specific capacity of 700 mAh g^{-1} at 2 C. J. He [20] prepared sulphur wrapped by N-doped graphene nanosheets using a simple spray drying method. The obtained composite demonstrates a good cycling stability performance, indicating that the unique wrinkled architecture not only prevents the dissolution of lithium polysulphides in the electrolyte but also accommodates volume expansion during the charge and discharge cycling process. These results suggest that graphene is a potential sulphur host material in Li/S batteries that can be easily modified to enhance its properties by doping with heterogeneous atoms [21-23]. Thirumal's group studied an effective approach to the synthesis of boron doped graphene nanosheets for supercapacitor applications that provides high capacitance and energy density [24]. However, there has been very little research on the application of Li/S batteries.

Herein, we adopt a facile hydrothermal synthesis method to prepare boron-doped reduced graphene oxide (B-rGO) material as a carbon matrix in a sulphur cathode and prepare S/B-rGO composites via the calcinations progress in a tubular furnace under an argon atmosphere. Finally, the physical properties of the S/B-rGO composite are investigated by different characteristic analyses. In addition, the electrochemical performance of the S/B-rGO composite as cathode material for Li/S batteries is examined and discussed. The results show that successful boron doping on the reduced graphene oxide not only improves the electric conductivity of the composite cathode but also retards the shuttle effect, which effectively demonstrates excellent cycling stability and rate capability.

2. EXPERIMENT

First, graphene oxide (GO) was synthesized from natural graphene powder via the modified Hummers method reported previously [25-27]. Second, B-rGO was obtained by a facile hydrothermal synthesis method. In brief, the prepared GO suspension was mixed with 200 mg boric acid and 8 ml ethanol by sonication for 20 min. Third, the mixture solution was poured into a sealed Teflon-lined 50 ml autoclave and heat treated at 180 °C for 12 h, resulting in a B-rGO hydrogel, followed by washing with deionized water five times. B-rGO was obtained by freeze drying in a vacuum oven at 60 °C for 24 h. Finally, B-rGO materials were added to a nano-sulphur aqueous suspension and sonicated for 2 h. After further vacuum drying, the suspension mixture was calcined in a tubular furnace under an argon atmosphere at 150 °C for 6 h.

The surface morphologies were observed by scanning electron microscopy (SEM, JSM-7610F, JOEL). X-ray diffraction (XRD) patterns were detected by an X-ray diffractometer (D8 Advance, Bruker) with Cu Kα radiation. Thermo-gravimetric analyses (TGA) were determined using a thermogravimetric analyser (SDT Q-600, TA) under N_2 gas. Raman spectra were obtained using a Raman spectrometer (inVia Reflex, Renishaw) from 100 cm^{-1} to 2500 cm^{-1}. Fourier transform infrared (FT-IR) spectra were measured using KBr pellets and an FT-IR spectrometer (V80, Bruker). The

microstructure of the sample was characterized by a transmission electron microscope (TEM, JEM-2010FEF, JOEL).

The electrochemical performance of the S/B-rGO composite cathode was measured using coin-type cells (CR2025). The cells were fabricated by sandwiching a microporous polypropylene separator between the S/B-rGO composite cathode and lithium metal anode. The electrolyte was 1 M lithium bis (trifluoromethane) sulphonamide (LiTFSI) mixed with 1,2-dioxolane (DOL) and dimethoxymethane (DME) (1:1 by volume). The cells were tested using a Neware battery testing system between 1.5 V and 3 V (vs. Li/Li^+). Cyclic voltammetry (CV) was performed on a Princeton Versa STAT4 electrochemical workstation between 1.5 V and 3 V. The electrochemical impedance spectroscopy (EIS) measurement was performed between 0.1 Hz and 100 kHz.

3. RESULTS AND DISCUSSION

Figure 1 shows the XRD patterns of elemental sulphur present in its characteristic orthorhombic crystal structure. These peaks are also obviously present in the S/B-rGO composite but with reduced intensity, which indicates the well-dispersed character of elemental sulphur in the S/B-rGO composite crystal structure. The typical diffraction peak of graphene is centred at 26° and corresponds to the (002) plane [28-29]. As seen from Fig. 1, the diffraction peak near 26° in the S/B-rGO composite is of low intensity, which can be attributed to the well-dispersed S/B-rGO composite using the one-pot hydrothermal synthesis method. The results indicate that a homogeneous mixture of the S/B-rGO composite was obtained in this investigation.

As shown in Fig. 2, the TGA curves of the S/B-rGO composite were studied using thermo-gravimetric analyses in a nitrogen atmosphere. Due to the sublimation of encapsulated sulphur, the primary weight loss of sulphur occurred between 200 °C and 300 °C. Because of this weight loss, the sulphur content in the S/B-rGO composite was tested at approximately 73.84%, which is much higher than that reported in many papers in recent years [30-32].

The Raman spectra of the S/B-rGO composite exhibit a small peak at approximately 470 cm^{-1} in Fig. 3, which is ascribed to the characteristic peak of S_8 [33]. One graphitic sp^2 hybridized G band appears at approximately 1590 cm^{-1} and another strong high intensity disorder D band appears at approximately 1350 cm^{-1} [34]. We can easily observe that the high intensity ratio of D band to G band (I_D/I_G) is 1.21, which indicates that the structural disorder of graphene increases upon boron doping.

The functional groups of the S/B-rGO composite were analysed by FT-IR between 500 and 4000 cm^{-1} as shown in Fig. 4. FT-IR spectra of the S/B-rGO composite showed that the two peaks centred at 1049 cm^{-1} and 1162 cm^{-1} correspond to asymmetric B-O stretching and C-O stretching, respectively. The B-C stretch at 1116 cm^{-1} indicates boron doping in the carbon network [35]. In addition, the peak (3451 cm^{-1}) is due to the O-H stretching vibration [36]. These functional groups in the S/B-rGO composite indicate that boron atoms were successfully doped in the structure of the carbon atoms network [37].

The morphology of the S/B-rGO composite was investigated by SEM. The image in Fig. 5 (a) presents a two-dimensional (2D) graphene-like structure of a few hundred nanometres in size. Boron

doping is positively polarized, so it can chemically adsorb negative species on the surface of a carbon framework [38-39]. The TEM image of the S/B-rGO composite shows a restacked structure in Fig. 5 (b). With the comprehensive analysis of SEM and TEM images, the S/B-rGO composites can improve the conductivity of electrode materials. Longer polysulphide diffusion not only has space to compensate for physical volume changes during charging and discharging cycles but also to improve physical polysulphide trapping ability [40-41]. In addition, the 2D stacked composites lead to greater reuse of the active material, longer polysulphide diffusion paths and improved conductivity of electrode materials.

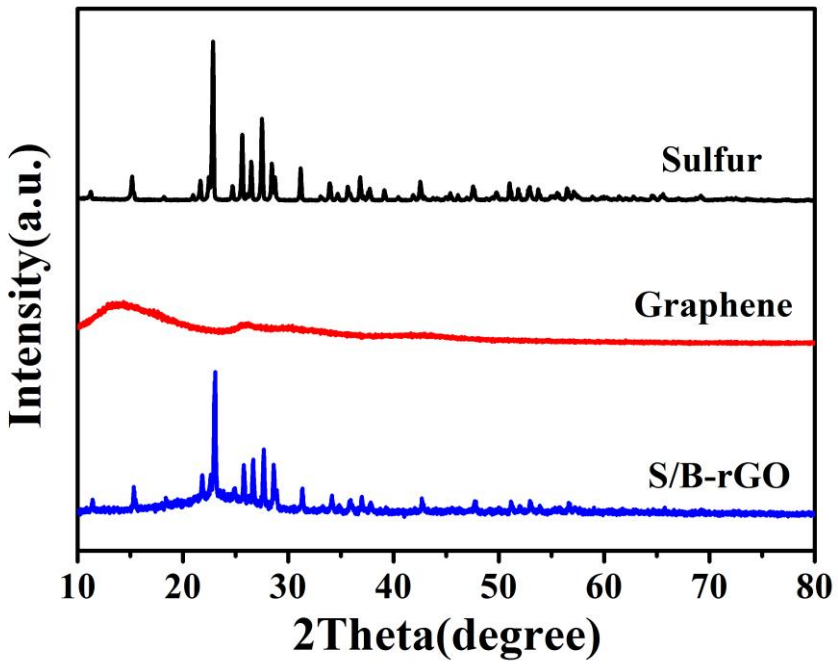

Figure 1. XRD patterns of elemental sulphur, graphene and the S/B-rGO composite.

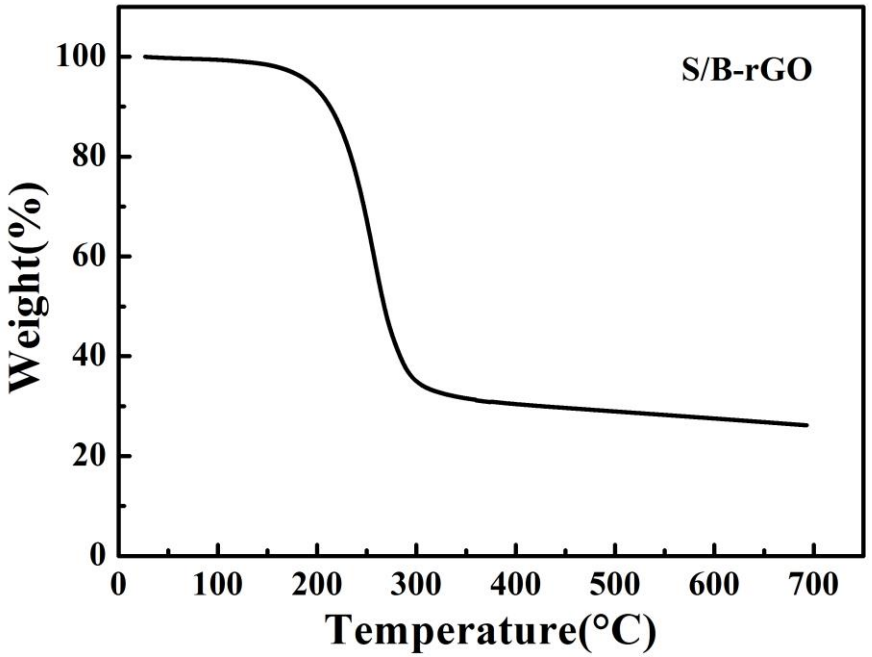

Figure 2. Thermogravimetric curve of the S/B-rGO composite in a nitrogen atmosphere with a heating rate of 10 °C min^{-1}.

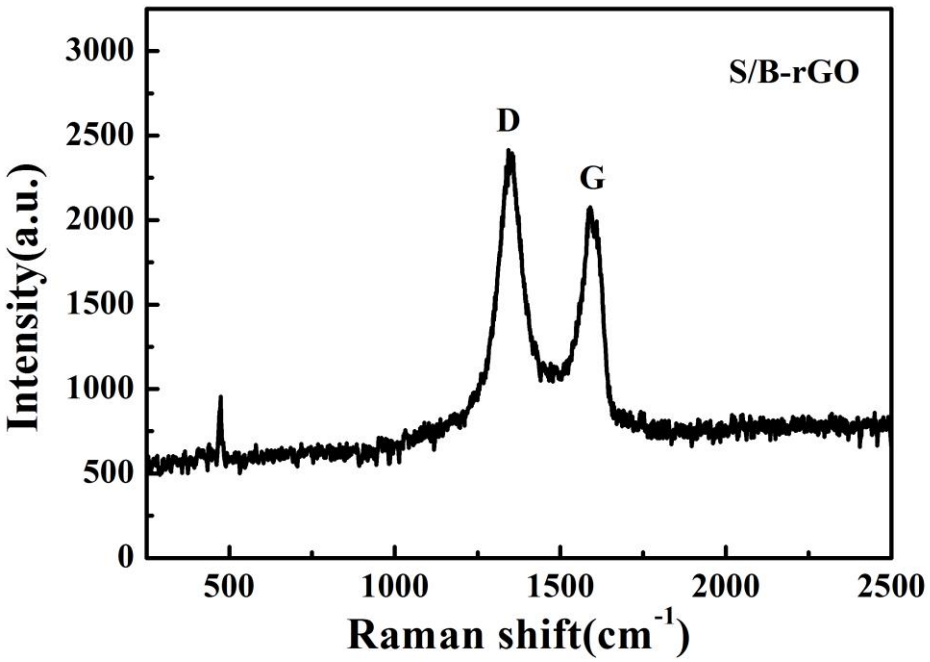

Figure 3. Raman spectra of the S/B-rGO composite.

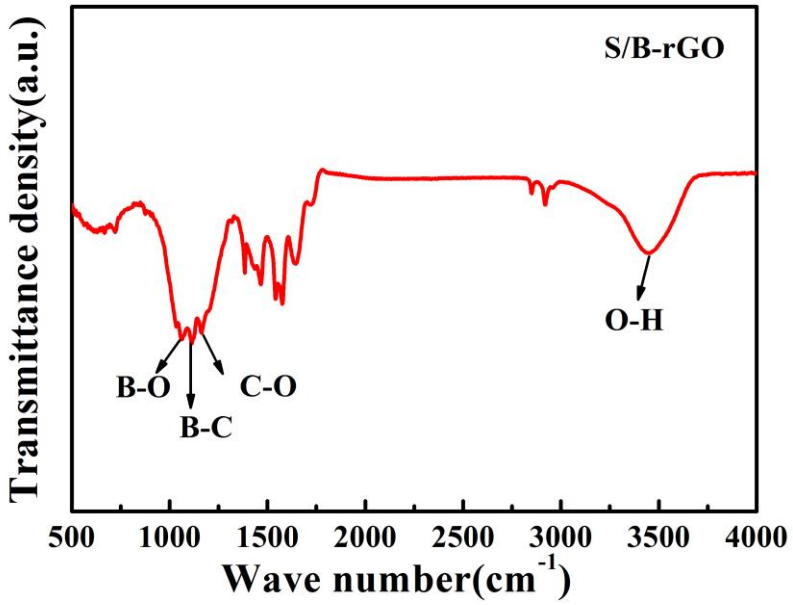

Figure 4. FT-IR spectra of the S/B-rGO composite.

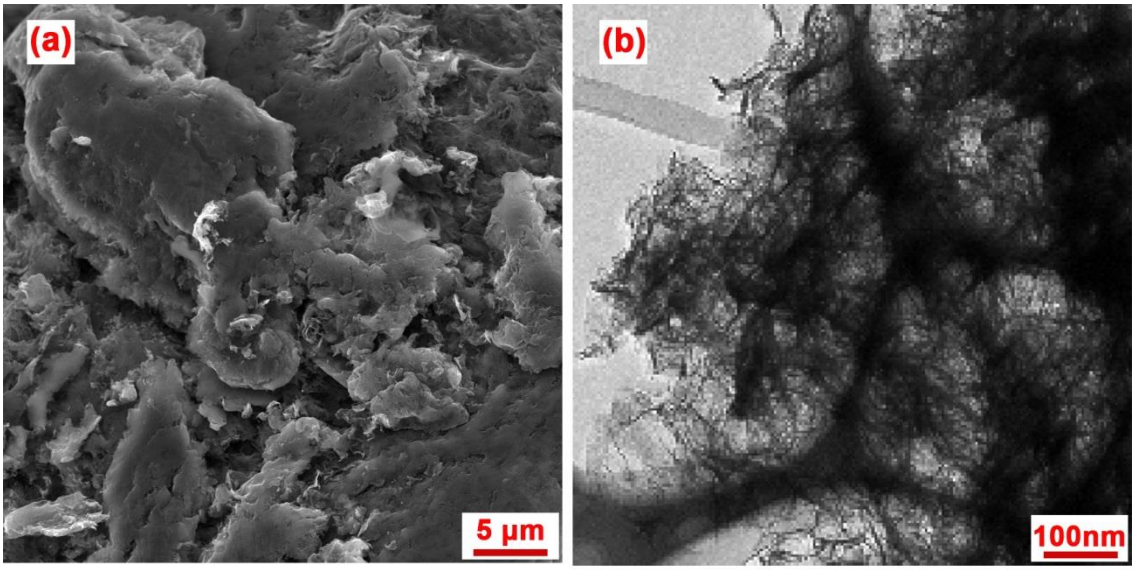

Figure 5. (a) SEM image of the S/B-rGO composite; **(b)** TEM image of the S/B-rGO composite.

To further explain the effect of boron doping in the composite, the XPS spectra of B 1s and S 2p were detected. As seen from Fig. 6 (a), the B 1s peak (~190 eV) demonstrates successful boron doping on the reduced graphene oxide. At the same time, the four peaks at 187.3 eV, 190.3 eV, 191.9 eV and 192.6 eV in Fig. 6 (b) originated from the presence of B, -BC_3, -BCO_2 and -BC_2O bonds [42], respectively, which indicates that boron atoms successfully combined with the carbon skeleton in different forms. Fig. 6 (c) shows the S 2p spectra of the S/B-rGO and sulphur/reduced graphene oxide

(S/rGO) composites; the sulphur bonding energy of the S/B-rGO composite is higher, revealing the stronger chemical interaction between sulphur and boron-doped reduced graphene oxide [43-44].

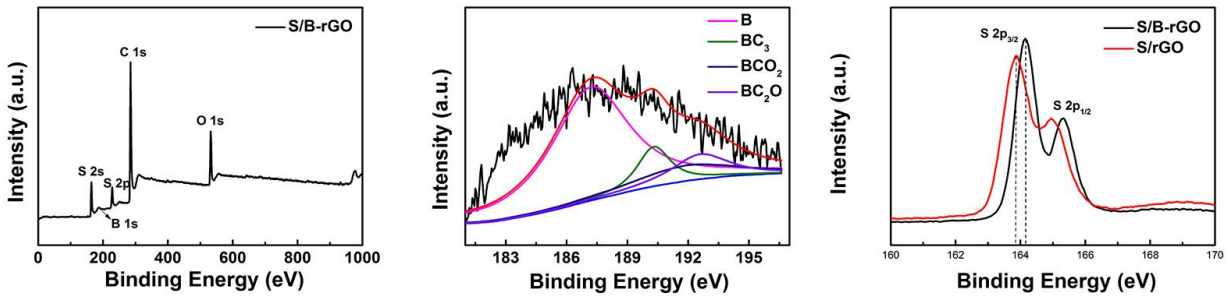

Figure 6. (a) XPS spectrum; **(b)** B 1s spectrum of the S/B-rGO composite; **(c)** S 2p spectra of the S/B-rGO and S/rGO composites.

The electrochemical performance of the S/B-rGO cathode composite was evaluated. Fig. 7 (a) shows several CV curves of the S/B-rGO cathode composite at a scanning rate of 0.1 mV s^{-1} between 1.5 V and 3 V. The two discernable reductive peaks in the CV curves can be ascribed to the transformation of sulphur to high-order polysulphides of Li_2S_n ($4 \leq n \leq 8$) and further reduction to Li_2S_2 or Li_2S. The prominent oxidation peak observed in Fig. 7 (a) is due to the complete conversion of Li_2S and Li_2S_n ($4 \leq n \leq 8$) into sulphur. Starting with the second cycling, the current and potential of the redox peaks remain almost unchanged, which indicates an excellent reactive reversibility and cycling stability. The electrochemical performance of the S/B-rGO composite cathode was further tested by galvanostatic charge and discharge cycling at 0.1 C between 1.5 V and 3 V. As shown in Fig. 7 (b), there are two typical plateaus in the discharge curve that can be assigned to the two reduction peaks. Moreover, the second plateau is very flat, suggesting a uniform deposition of Li_2S [45]. Moreover, the discharge and charge profiles of the S/B-rGO and S/rGO composites after 100 cycles at 0.1 C are shown in Fig. 7 (b). The S/B-rGO composite maintains a high reversible discharge capacity of approximately 521.9 mAh g^{-1} after 100 cycles at 0.1 C, compared to 270 mAh g^{-1} for the S/rGO composite. Hence, the introduction of boron-doping reduced oxide graphene benefits the low electric conductivity of the cathode and consequently improves the energy density of the batteries .

As illustrated in Fig. 7 (c), the cycle performances of the S/B-rGO and S/rGO composites were tested for 100 cycles. The S/B-rGO composite exhibited enhanced electrochemical performance, whereas the S/rGO composite had a capacity fading for charge/discharge cycling. Such an excellent cycle performance is much better than that of many 2D graphene-sulphur cathode materials [46-48] and is superior to many of the 3D graphene-sulphur materials with un-doped impurity atoms [49-50].

The rate capability results presented excellent performances by the S/B-rGO cathode composite compared to the S/rGO cathode composite at a variety of current rates, as shown in Fig. 7 (d). Average reversible capacities of 632.89, 541.12, 487.99, 437.98 and 384.73 mAh g^{-1} were obtained at initial cycles for the S/B-rGO cathode composite at current rates of 0.1 C, 0.2 C, 0.5 C, 1 C and 2 C, respectively. When the current rate dropped from 2 C to 0.1 C, the discharge capacity of the S/B-rGO cathode composite was mostly recovered. The excellent high-rate performance is ascribed to the good

electrical conductivity of B-rGO as an effective electron conduction path in the sulphur electrode. Such results show that the S/B-rGO cathode composite materials not only provide a stable and continuous pathway for rapid electron and ion transportation but also maintain the integrity of cathode materials and accommodate the volume change caused by sulphur during the cycling process. In addition, the excellent rate capability also benefits from the preparation of B-rGO by a facile hydrothermal synthesis method, as indicated by the following EIS analysis.

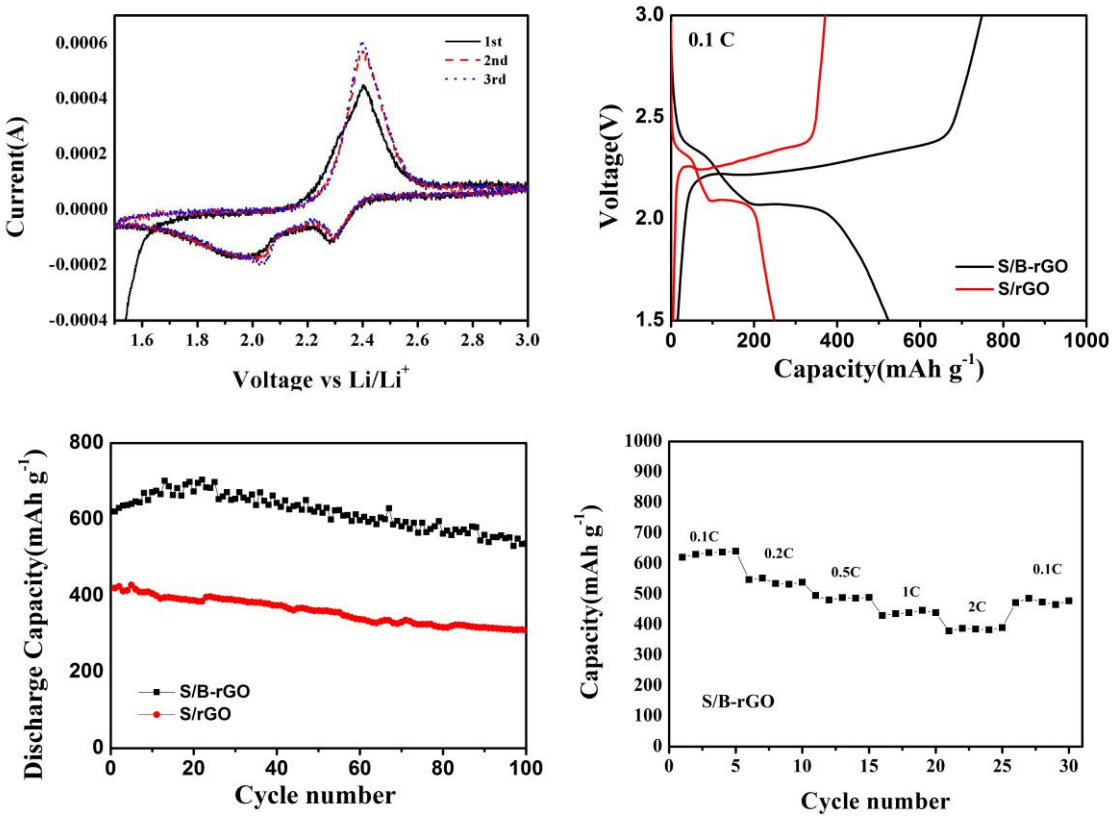

Figure 7. Electrochemical performance of Li/S batteries. **(a)** Cyclic voltammograms with the S/B-rGO cathode composite at a 0.1 mV s^{-1} scan rate; **(b)** Charge and discharge profiles with the S/B-rGO cathode composite and the S/rGO cathode composite after 100 cycles at 0.1 C; **(c)** Cycling performance of the S/B-rGO cathode composite and S/rGO cathode composite at 0.1 C; **(d)** Rate capability of the S/B-rGO cathode composite.

To further confirm the good electrochemical performance of the S/B-rGO cathode composite, we conducted EIS measurements after the first charge and discharge cycling at 0.1 C, as shown Fig. 8. Both composite cathodes are composed of a semicircle in the middle-frequency region and a short-sloped line in the low-frequency region corresponding to the slow reaction kinetics of Li_2S and Li_2S_2 [51]. The smaller semicircle, related to the lower charge transfer resistance of the S/B-rGO cathode composite, indicates that the introduction of boron-doped reduced oxide graphene can improve electronic conductivity and provide a mechanically flexible framework, which explains the electrochemical performance enhancement for Li/S batteries.

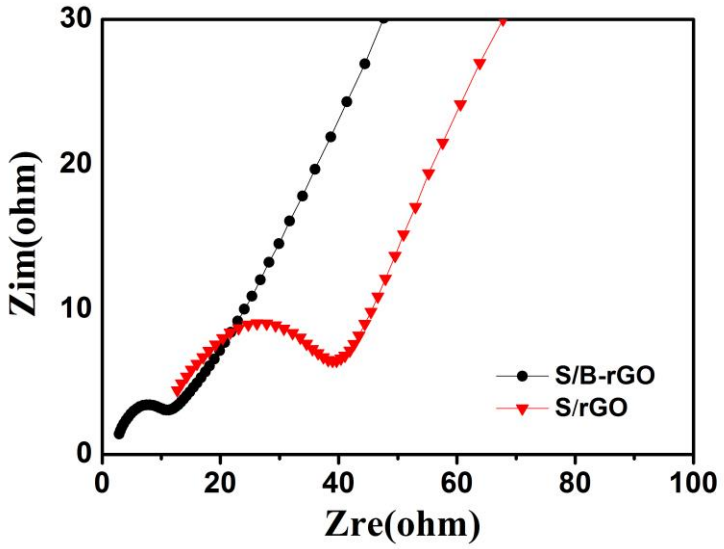

Figure 8. EIS impedance plots of Li/S batteries with the S/B-rGO cathode composite and S/rGO cathode composite after the first charge/discharge cycle.

4. CONCLUSIONS

A facile hydrothermal synthesis method for fabricating a boron-doped reduced graphene oxide/sulphur composite has been developed. A two-dimensional stacked nanosheets structure was formed in the S/B-rGO composite. Therefore, the S/B-rGO composite exhibited an enhanced cyclability and improved rate capability as cathode material for Li/S batteries. Furthermore, the present synthesis strategy provides a simple route for synthesizing a well-dispersed B-rGO composite that can act as an electron conductor, thus significantly improving the electrochemical properties. Therefore, the S/B-rGO composite is a potential cathode material for high-performance Li/S batteries.

ACKNOWLEDGEMENTS
The authors acknowledge the financial support from the National Natural Science Foundation of China (Grant No. 21406052), the Program for the Outstanding Young Talents of Hebei Province (Grant No. BJ2014010), Scientific Research Foundation for Selected Overseas Chinese Scholars, Ministry of Human Resources and Social Security of China (Grant No. CG2015003002).

References

1. B. Kang, G. Ceder, *Nature*, 458 (2009) 190.
2. A. Mentbayeva, A. Belgibayeva, N. Umirov, Y.G. Zhang, I. Taniguchi, I. Kurmanbayeva, Z. Bakenov, *Electrochim. Acta*, 217 (2016) 242.
3. Y. Zhao, Y.G. Zhang, D. Gosselink, T.N.L. Doan, M. Sadhu, H.J. Cheang and P. Chen, *Membranes*, 2 (2012) 553.
4. K. Byoungwoo and C. Gerbrand, *Nature*, 458 (2009) 190.
5. A. Konarov, D. Gosselink, T.N.L. Doan, Y.G. Zhang, Y. Zhao and P. Chen, *J. Power Sources*, 259 (2014) 183.
6. P.G. Bruce, S.A. Freunberger, L.J. Hardwick and J.M. Tarascon, *Nat. Mater*., 11 (2012) 19.

7. Y.G. Zhang, Z. Bakenov, Y. Zhao, A. Konarov, T.N.L. Doan, K.E.K. Sun, A. Yermukhambetova and P. Chen, *Powder Technol*., 235 (2013) 248.
8. M.D. Patel, E. Cha, C. Kang, B. Gwalani and W. Choi, *Carbon*, 118 (2017) 120.
9. W. Ahn, K.B. Kim, K.N. Jung, K.H. Shin and C.S. Jin, *J. Power Sources*, 202 (2012) 394.
10. L.W. Ji, M.M. Rao, S. Aloni, L. Wang, E.J. Cairns and Y.G. Zhang, *Energy Environ. Sci*., 4 (2011) 5053.
11. H.P. Li, Y. Li, Y.G. Zhang, C.W. Zhang, *J. Nanopart. Res*., 17 (2015) 370.
12. J.Z. Chen, D.X. Wu, E. Walter, M. Engelhard, P. Bhattacharya, H.L. Pan, Y.Y. Shao, F. Gao, J. Xiao and J. Liu, *Nano Energy*, 13 (2015) 267.
13. Z. Li, Y. Jiang, L.X. Yuan, L.X. Yi, Z.Q. Yi, C. Wu, Y. Liu, P. Strasser and Y.H. Huang, *ACS Nano*, 8 (2014) 9295.
14. L.C. Yin, J.L. Wang, F.J. Lin, J. Yang and Y. Nuli, *Energy Environ. Sci*., 5 (2012) 6966.
15. C.X. Zu and A. Manthiram, *Adv. Energy Mater*., 3 (2013) 1008.
16. S.T. Lu, Y. Chen, X.H. Wu, Z.D. Wang and Y. Li, *Sci. Rep*., 4 (2014) 4629.
17. Y.G. Zhang, Y. Zhao, A. Konarov, D. Gosselink, H.G. Soboleski, P. Chen, *J. Power Sources*, 241 (2013) 517.
18. X. Yang, L. Zhang, F. Zhang, Y. Huang and Y.S. Chen, *ACS Nano*, 8 (2014) 5208.
19. A. Konarov, Z. Bakenov, H. Yashiro, Y.K. Sun and S.T. Myung, *J. Power Sources*, 355 (2017) 140.
20. J. He, K. Zhou, Y. Chen, C. Xu, J. Lin and W. Zhang, *Mater. Today Energy*, 1-2 (2016) 11.
21. Z.S. Wu, W. Ren, L. Xu, F. Li and H.M. Cheng, *ACS Nano*, 5 (2011) 5463.
22. Y. Liu, P. Liu, D. Wu, Y. Huang, Y. Tang, Y. Su, F. Zhang and X. Feng, *Chem. Eur. J.*, 21 (2015) 5617.
23. B. Jiang, C. Tian, L. Wang, L. Sun, C. Chen, X. Nong, Y. Qiao and H. Fu, *Appl. Surf. Sci*., 258 (2012) 3438.
24. V. Thirumal, A. Pandurangan, R. Jayavel and R. Ilangovan, *Synth. Met*., 220 (2016) 524.
25. W.S. Hummers and R. Offrman, *J. Am. Chem. Soc*., 80 (1958) 1339.
26. R.E.O. William, S. Hummers Jr. 208 (1957) 1937.
27. M.G. Kim and J. Cho, *Adv. Fun. Mater*., 19 (2009) 1497.
28. L.G. Bulusheva, A.V. Okotrub, A.G. Kurebya, H.K. Zhang, H.J. Zhang, X.H. Chen and H.H. Song, *Carbon*, 49 (2011) 4013.
29. X. Lin, X. Lu, T. Huang, Z. Liu and A. Yu, *J. Power Sources*, 242 (2013) 855.
30. Y. Zhao, Z. Bakenova, Y.G. Zhang, H.P. Li, H.X. Xie and Z. Bakenov, *Ionics*, 21 (2015) 1925.
31. J. Zhang, Z.M. Dong, X.L. Wang and G.H. Du, *J. Power Sources*, 270 (2014) 1.
32. X. Yang, W. Zhu, G. Cao and X.F. Zhao, *Rsc Adv*., 6 (2016)7159.
33. Z.S. Wu, A. Winter, L. Chen, Y. Sun, A. Turchanin, X. Feng and K. Müllen, *Adv. Mater*., 24 (2012) 5130.
34. R. Vaidhyanathan, S.S. Iremonger, G.K.H. Shimizu, P.G. Boyd, S. Alavi and T.K. Woo, *Angew. Chem. Int. Ed.*, 51 (2012) 1826.
35. H. Wehrheit, T. Au, R. Schmechel, S.O. Shalamberidze, G.I. Kalandadze and A.M. Eristavi, *J. Solid State Chem*., 154 (1999) 79.
36. L. Wang, Y.J. Ye,; X.P. Lu, Z.B. W en, Z. Li, H.Q. Hou and Y.H. Song, *Sci. Rep*., 3 (2013) 3568.
37. V. Thirumal, A. Pandurangan, R. Jayavel and R. Iiangovan, *Synthetic Met*., 220 (2016) 524.
38. C.P. Yang, Y.X. Yin, H. Ye. K.C. J iang, J. Zhang and Y.G. Guo, *ACS Appl. Mater. Interfaces*, 6 (2014) 8789.
39. L. Yang, S. Jiang, Y. Zhao, L. Zhu, S. Chen, X. Wang, Q. Wu, J. Ma, Y. Ma and Z. Hu, *Angew. Chem. Int. Ed.*, 50 (2011)7132.
40. I. Mukhopadhyay, N. Hoshino, S. Kawasaki, F. Okino, W.K. Hsu and H. Touhara, *J. Electrochem. Soc*., 149 (2002) A39.
41. L.S. Panchakarla, K.S. Subrahmanyam, S.K. Saha, A. Govindaraj, H.R. Krishnamurthy, U.V. Waghmare and C.N.R. Rao, *Adv. Mater*., 21 (2009) 4726.

42. T.V. Vineesh, M.P. Kumar, C. Takahashi, G. Kalita, S. Alwarappan, D.K. Pattanayak and T.N. Narayanan, *Adv. Energy Mater*., 5 (2015) 1500658.
43. Y. Xie, Z. Meng, T. Cai and W.Q. Han, *ACS Appl. Mater. Interfaces*, 7 (2015) 25202
44. C.P. Yang, Y.X. Yin, H. Ye, K.C. Jiang, J. Zhang and Y.G. Guo, *ACS Appl. Mater. Interfaces*, 6 (2014) 8789.
45. T.Q. Lin, Y.F. Tang, Y.M. Wang, H. Bi and Z.Q. Liu, *Energy Env. Sci*., 6 (2013) 1283.
46. G.M. Zhou, L.C. Yin, D.W. Wang, L. Li, S.F. Pei, I.R. Gentle, F. Li and H.M. Cheng, *ACS Nano*, 7 (2013) 5367.
47. M. Endo, K. Takeuchi, T. Hiroka, T. Furuta, T. Kasai, X. Sun and C.H. Kiang, *Chem. Solids*, 58 (1997) 1707.
48. X.F. Gao, J.Y. Li, D.S. Guan and C. Yuan, *Acs Appl. Mater. Interfaces*, 6 (2014) 4154.
49. C.M. Xu, Y.S. Wu, X.Y. Zhao, X.L. Wang, G.H. Du, J. Zhang and J.P. Tu, *J. Power Sources*, 275 (2015) 22.
50. D.H. Wang, X.H. D. Xie, X.Q. Niu, X. Ge, C.D. Gu, X.L. Wang and J.P. Tu, *J. Power Sources*, 299 (2015) 293.
51. T.N.L. Doan, M. Ghaznavi, A. Konarov, Y.G. Zhang and P. Chen, *J. Solid State Electrochem.*, 18 (2014) 69.